

Accelerating relaxation through Liouvillian exceptional point

Yan-Li Zhou,^{1,2,3} Xiao-Die Yu,⁴ Chun-Wang Wu,^{1,2,3} Xie-Qian Li,¹ Jie Zhang,^{1,2,3} Weibin Li,^{5,*} and Ping-Xing Chen^{1,2,3,†}

¹*Institute for Quantum Science and Technology, College of Science, National University of Defense Technology, Changsha 410073, China*

²*Hunan Key Laboratory of Mechanism and technology of Quantum Information, Changsha 410073, China*

³*Hefei National Laboratory, Hefei 230088, Anhui, China*

⁴*College of Science, National University of Defense Technology, Changsha 410073, China*

⁵*School of Physics and Astronomy, and Centre for the Mathematics and Theoretical Physics of Quantum Non-equilibrium Systems, University of Nottingham, Nottingham NG7 2RD, United Kingdom*

We investigate speeding up of relaxation of Markovian open quantum systems with the Liouvillian exceptional point (LEP), where the slowest decay mode degenerate with a faster decay mode. The degeneracy significantly increases the gap of the Liouvillian operator, which determines the timescale of such systems in converging to stationarity, and hence accelerates the relaxation process. We explore an experimentally relevant three level atomic system, whose eigenmatrices and eigenspectra are obtained completely analytically. This allows us to gain insights in the LEP and examine respective dynamics with details. We illustrate that the gap can be further widened through Floquet engineering, which further accelerates the relaxation process. Finally, we extend this approach to analyze laser cooling of trapped ions, where vibrations (phonons) couple to the electronic states. An optimal cooling condition is obtained analytically, which agrees with both existing experiments and numerical simulations. Our study provides analytical insights in understanding LEP, as well as in controlling and optimizing dissipative dynamics of atoms and trapped ions.

I. INTRODUCTION

Open quantum systems coupled to environments will relax toward a stationary state. The relaxation processes have rich properties from both dynamic and thermodynamic perspectives. Often an important question is to control the relaxation time [1–4], for instance, on a timescale as short as possible [see Fig. 1(a)]. This problem is of great relevance to cases where one is concerned with properties of stationary states, such as ground state laser cooling [5–9], or aims to generate quantum states for quantum applications [10–13].

Starting from an arbitrary initial state, the relaxation timescale is largely characterized by the slowest decay mode of the Liouvillian operator. The gap is defined as modulus of the real part of its eigenvalue λ_1 [14–16], as depicted in Fig. 1(b). Therefore, relaxation speeding is achieved through increasing the gap. An alternative approach to speed the relaxation is offered by the so-called Mpemba effect [17–20], where an unitary operation on the initial pure state removes its overlap with the slowest decaying mode [1, 2]. This transformation can be exactly constructed provided that the initial state is a pure state.

In this paper, we show that, for an arbitrary initial state, if the slowest decay mode and its corresponding eigenvalue coalesce with a faster decay mode, one can maximize the gap and thus accelerates dynamics to reach stationary states. Our study exploits the novel nature of

exceptional points (EPs), which are hallmarks of non-Hermitian systems [21–28]. EPs are specific points in parameter space, where two or more eigenvalues of a non-Hermitian operator and their corresponding eigenvectors coalesce [29]. The origin of non-Hermiticity is the coupling between the system and the environment. Liouvillian superoperator, which captures the time evolution of an open quantum system, is non-Hermitian. Therefore, it can exhibit EPs (referred to as Liouvillian EPs, or LEPs) [24, 29]. Properties of LEPs, with diverse unusual effects, have attracted considerable attention currently [30–32], such as dissipative phase transition [33–35], non-Hermitian skin effect [36], signatures of LEPs in the dynamics [37–39] and so on.

Here, we focus on analytical understanding and applications of LEPs in quantum control [40, 41], and further explore how to accelerate the relaxation towards to stationarity in Markovian open quantum systems via LEPs. The basic mechanism underpinning our study is based on the fact that, at LEPs both the slowest decay mode and corresponding eigenvalue coalesce with a faster decay mode and the corresponding eigenvalue. We show that, when the stationary state of the system is unique and independent on system parameters, one can set the parameters at the LEP to speed up the relaxation process significantly. For certain quantum dynamic processes, such as ground state cooling, how to convergent to stationarity as quickly as possible is often a concern in the actual process of quantum manipulation. In addition, we find that relaxation processes can be further accelerated by periodically modulating the dissipation strength, i.e., the Floquet modulation can overcome the gap limit of the static case and realize faster relaxation [see Fig. 1(c)

* weibin.li@nottingham.ac.uk

† pxchen@nudt.edu.cn

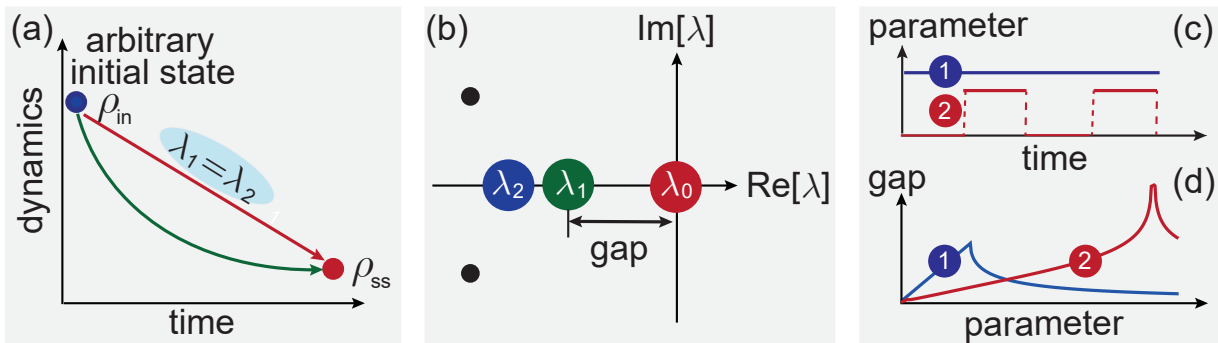


Figure 1. (a) For an open quantum system with an arbitrary initial state, the timescale of approaching to the final stationary state ρ_{ss} is related to the slowest decay mode (with eigenvalue λ_1) of Liouvillian superoperator. By tuning the parameter of the system near the LEPs, where both of the slowest decaying mode and the corresponding eigenvalue are merged with a faster decaying mode and the corresponding eigenvalue (for instance λ_2), the system dynamics approaches the stationary state in a much faster way. (b) This feature is evident from the Liouvillian spectrum. The stationary state ρ_{ss} is characterized by the largest eigenvalue $\lambda_0 = 0$. The other eigenvalues, characterizing the decay modes, have non-positive real part and always appear as complex conjugates. The Liouvillian spectral gap ($g = -\text{Re}[\lambda_1]$) determines the relaxation timescale, and can reach its maximum value at LEP. (c-d) The gap at LEP can be further increased by the Floquet method (Red line). In contrast with the static case (Blue line), the gap under time-periodic modulation can be significantly increased, which means that relaxation process will be accelerated by applying the Floquet method.

d)]. We apply our approach to analyze ground state laser cooling based on sideband transitions and electromagnetically induced transparency (EIT). Optimal conditions are obtained analytically, which have been demonstrated in recent trapped ion experiments [7, 9]. Our study reveals the importance of LEPs in practical applications and provides insights in seeking optimal conditions in quantum control of open quantum systems.

This paper is organized as follows. In Sec. II, we introduce the master equation of the Markovian open quantum systems. A general framework that connects to its dynamics and eigenmatrices of the Liouvillian superoperator is provided. This provides an intuitive picture to understand the relaxation and the gap. In Sec. III, we study the dynamics of dissipative three-level system. Eigenmatrices and eigenvalues of the corresponding Liouvillian superoperator are obtained analytically. Based on the analytical calculation, we reveal that the relaxation towards to stationary state can be accelerated by exploiting static and Floquet-modulated LEPs. Next, in Sec. IV applications for ground state laser cooling are demonstrated. Two experimentally relevant scenarios, i.e. sideband cooling and EIT cooling, are examined. Optimal cooling conditions are obtained at corresponding LEPs. We conclude in Sec. V.

II. LIOUVILLIAN GAP, DYNAMICS AND LEP

We consider an open quantum system evolving under Markovian dynamics, governed by master equation $\dot{\rho}(t) = \mathcal{L}\rho(t)$, where the generator \mathcal{L} , normally called Li-

ouvillian superoperator, has the form [42, 43]

$$\mathcal{L}\rho = -i[H, \rho] + \sum_{\alpha} (J_{\alpha}\rho J_{\alpha}^{\dagger} - \frac{1}{2}\{J_{\alpha}^{\dagger}J_{\alpha}, \rho\}). \quad (1)$$

Here, $\rho(t)$ is the state of the system at time t , H is the system Hamiltonian, and J_{α} are quantum jump operators which provide coupling of the system to the environment. Since the Liouvillian \mathcal{L} acts linearly on $\rho(t)$, one can obtain information about the relaxation in terms of its eigenmatrices R_i and the corresponding complex eigenvalues λ_i via the relation $\mathcal{L}R_i = \lambda_i R_i$. Note that, due to the Hermiticity of \mathcal{L} , if λ_i is complex, λ_i^* must also be an eigenvalue of \mathcal{L} [1, 24, 34, 44]. Therefore, the eigenvalues are symmetrically distributed with respect to the real axis as shown in Fig. 1(b).

The stationary state of the system under consideration is then given by the density matrix ρ_{ss} such that $\mathcal{L}\rho_{ss} = 0$, i.e., $\rho_{ss} = R_0$, which corresponds to the zero eigenvalue $\lambda_0 = 0$ and is independent of the initial state. If the eigenvalues are ordered by decreasing their real parts, it is known that the negative real parts of the eigenvalues [45], $\text{Re}[\lambda_{i>0}] < 0$, determine the relaxation rates of the system towards the nonequilibrium stationary state, and the corresponding eigenmatrices $R_{i>0}$ are called decay modes [15, 46]. While the imaginary parts describe the oscillatory processes which may take place. We can then write the time dependence of the density operator from an initial state ρ_{in} as

$$\rho(t) = e^{\mathcal{L}t}\rho_{in} = \rho_{ss} + \sum_{i \geq 1} a_i e^{\lambda_i t} R_i, \quad (2)$$

where $a_i = \text{Tr}[L_i \rho_{in}]$ are coefficients of the initial state decomposition into the eigenmatrices of \mathcal{L}^{\dagger} with $\mathcal{L}^{\dagger} L_i =$

$\lambda_i^* L_i$. Here R_i and L_i are referred as right and left eigenmatrices (eigenmodes), respectively, and can be normalized by $\text{Tr}[L_i R_j] = \delta_{ij}$. The trace preservation of the dynamics implies that $\text{Tr}[\rho(t)] = \text{Tr}[\rho_{ss}] = 1 = \text{Tr}[L_0 R_0]$, and thus L_0 is the identity ($L_0 = I$). It also implies that $\text{Tr}[R_{i \geq 1}] = 0$, which means other right eigenmatrices do not correspond to quantum states. A particular interesting case is when eigenvalue λ_i is real, where the corresponding eigenmatrix can be diagonalized [34]. We can rewrite it as superposition of eigenstates from the diagonalization [34]

$$R_i \propto R_i^+ - R_i^-, \quad (3)$$

with

$$R_i^+ = \sum_n^{p_n \geq 0} p_n^i |\psi_n^i\rangle \langle \psi_n^i|, \\ R_i^- = \sum_n^{p_n < 0} p_n^i |\psi_n^i\rangle \langle \psi_n^i|, \quad (4)$$

where $|\psi_n^i\rangle$ are eigenvectors of R_i with eigenvalues p_n^i . With this definition, R_i^\pm are arranged to proper density matrices. If λ_i is complex, one can define a pair of eigenmatrices $R_i + R_i^\dagger$ and $i(R_i - R_i^\dagger)$, then their corresponding eigenvalues are real (i.e. real and imaginary parts of λ_i). This allows to diagonalize their new eigenmatrices.

A fundamental role in the system dynamics is played by $\lambda_1(R_1)$, which possesses the slowest decay rate on the condition $a_1 \neq 0$. Then the Liouvillian gap, defined by [14, 47]

$$g = |\text{Re}[\lambda_1]|, \quad (5)$$

is thus an important quantity determining the timescale of the final relaxation to the stationary state. If the slowest decay mode $\lambda_1(R_1)$ coalesce with a faster decay mode when we set the system parameters at the so-called LEP, where $\lambda_1(R_1) = \lambda_2(R_2)$, the gap will have extreme values g_{LEP} . Consequently for long times one has

$$\|\rho(t) - \rho_{ss}\| \propto e^{g_{\text{LEP}} t}, \quad (6)$$

where $\|A\| = \sqrt{\text{Tr}[AA^\dagger]}$ is the Hilbert-Schmidt distance. In such a case, the state would relax at the fastest rate with timescale $1/g_{\text{LEP}}$ for arbitrary initial state. As we will demonstrate latter, this is useful in some quantum applications, where long relaxation timescales become impractical or even harmful to the coherence. Therefore how to quickly approach the steady state becomes necessary in these applications.

III. ANALYTICAL LEP THEORY OF DISSIPATIVE THREE-LEVEL SYSTEM

A. The model

Consider a simple dissipative three-level system of Fig. 2(b). The state $|b\rangle$ resonantly couples to state $|c\rangle$ with

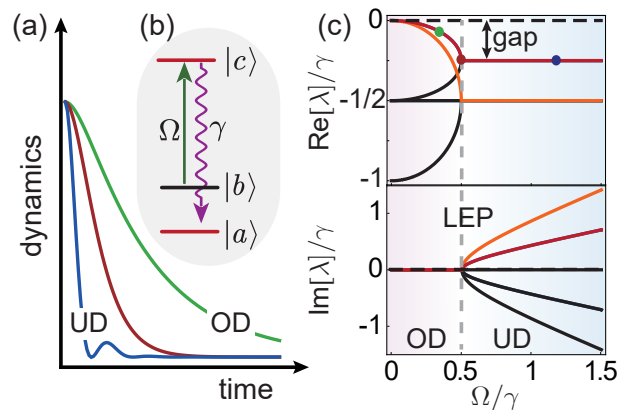


Figure 2. (a) Relaxation process. The system decays exponentially to the final stationary state. The numerical integration is performed in the under-damped (UD) regime for $\Omega/\gamma = 0.3$ (Green line), in the over-damped (OD) regime with $\Omega/\gamma = 1.2$ (Blue line), and in the LEP $\gamma/\Omega = 2$ (Red line). (b) Schematic of the system, γ denotes the emission rate of the $|c\rangle$ level to $|a\rangle$ level, and Ω denotes the coupling rate from an resonant drive between transition $|b\rangle$ - $|c\rangle$. (c) Real and imaginary parts of the Liouvillian spectra of the three-level system shown in (b). The dashed black line corresponds to $\lambda_0 = 0$. The red-lines corresponds λ_1 . The Liouvillian gap is denoted by $-\text{Re}[\lambda_1]$, and the LEP is indicated with a vertical dashed line.

Rabi frequency Ω , state $|c\rangle$ decays to state $|a\rangle$ with decay rate γ . This process results in state $|b\rangle$ decoupled from the coherent collective evolution and finally decay to the stationary state $|a\rangle$. For the model under consideration, we have the Hamiltonian

$$H = \frac{\Omega}{2}(|b\rangle\langle c| + |c\rangle\langle b|) \quad (7)$$

and a jump operator $J = \sqrt{\gamma}|a\rangle\langle c|$. Qualitatively, there will be competition between the reversible coherent coupling between $|b\rangle \leftrightarrow |c\rangle$ at frequency Ω and the population loss of $|c\rangle$ at a rate γ . As shown in Fig. 2(a), if $\Omega \gg \gamma$, Rabi oscillations occur before $|c\rangle$ eventually decays to $|a\rangle$ and dynamics of the system exhibits damped oscillations, which corresponds to under-damped (UD) dynamics. At very long times, the probability in the state $|b\rangle$ tends towards zero since the system ends up in level $|a\rangle$. If, on the other hand, $\Omega \ll \gamma$, we expect an over-damped (OD) evolution for the probability of state $|b\rangle$, which tends exponentially towards zero. The level $|b\rangle$ is irreversibly damped via its coupling with the strongly relaxing level $|c\rangle$, which appears then as an environment for the level $|b\rangle$.

This regime provides a tunable dissipation channel [10–12, 39] and recently, it is widely used to simulate parity-time (\mathcal{PT})-symmetric Hamiltonians with postselection of the jump results [28, 30, 48]. It can also describe the dynamics of the simplest situation of spin-spring system with relaxation processes[49]. For instance the damped vacuum Rabi oscillation by the state definition $|a\rangle =$

$|g, 0\rangle, |b\rangle = |e, 0\rangle$ and $|c\rangle = |g, 1\rangle$, where states $|a\rangle$ and $|b\rangle$ are coherently coupled by the Jaynes–Cummings Hamiltonian, while $|b\rangle$ decays towards $|c\rangle$ at the rate γ . Further more, as we will show below that, this simple model is the core physical principle of phonon ground state cooling [5, 50].

B. The Liouvillian spectra and LEPs

For this level system, the stationary state of the system is always $|a\rangle$ no matter how the initial state and parameters of the system change. If the goal is to prepare or use this state for related applications, it is unnecessary and even harmful to wait for a long relaxation timescales. In this instance, the most practical construction is to set the optimal parameters to ensure the approaching the stationary state on a timescale which is as short as possible. It can be obtained quantitatively by solving the spectrum of Liouvillian superoperator \mathcal{L} , as shown in Fig. 2(c), and it is $\{0, -(\gamma \pm \kappa)/4, -(\gamma \pm \kappa)/2, -\gamma/2\}$ with $\kappa = \sqrt{\gamma^2 - 4\Omega^2}$. Consequently, the spectrum gap is

$$g = \text{Re}\left[\frac{1}{4}(\gamma - \kappa)\right], \quad (8)$$

and it highlights three regimes for the dynamics as a function of Ω/γ as shown in Fig. 2(c). When $\Omega < \gamma/2$, \mathcal{L} exhibits a real spectrum, which means that all the excited eigenmodes exponentially decay with time, which corresponds to the OD regime. For $\Omega > \gamma/2$, on the other hand, \mathcal{L} exhibits a complex spectrum and the system still exhibits Rabi oscillations. For arbitrary initial state, it eventually is damped out with the effectively decay rate which is determined by the gap $g = \gamma/4$. This is UD regime. When $\Omega = \gamma/2$, two pairs of eigenvalues and eigenvectors of Liouvillian coalesce simultaneously (see Appendix A for the exact form of the eigensystem of Liouvillian \mathcal{L}), giving rise to two second-order and a third-order LEPs. It corresponds to a critical damping making the boundary between the OD and the UD regime [24, 38]. In particular, at LEP, the gap reaches the maximum value $g_{\text{max}} = \gamma/4 = \Omega/2$, corresponding to that the dynamics at the LEP situation is fastest.

As shown in Fig. 2(c), structures $\{-(\gamma \pm \kappa)/4\}$ and $\{-(\gamma \pm \kappa)/2, -\gamma/2\}$ of the spectrum reflect the two possible relaxation times of the system. Both of them get their minima value when $\kappa = 0$, $\lambda_{1(2)} = \lambda_{3(4)}$, $\lambda_5 = \lambda_6 = \lambda_7 = \lambda_8$, giving rise to two second-order and a third-order LEP. Note that when $\kappa = 0$, $R_1 = R_3$, $R_2 = R_4$, $R_5 = R_6 = R_7 \neq R_8$, which means that the corresponding eigenmatrix R_8 can not coalesce with $R_{5,6,7}$. Therefore, λ_8 does not play a role in the $\kappa = 0$ LEP.

In order to investigate the physical connotations of the two types of LEPs, we reduce the master equation to the non-zero matrix elements of ρ ,

$$\dot{\rho}_{bb} = i\frac{\Omega}{2}(\rho_{bc} - \rho_{cb}), \quad (9a)$$

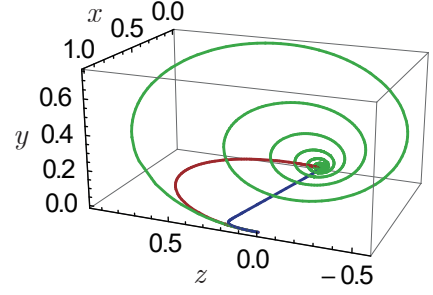


Figure 3. The dynamics of x, y, z . Green line: oscillatory regime for $\gamma = 0.2\Omega$, Red line: LEP for $\gamma = 2\Omega$ and Blue line: overdamped regime for $\gamma = 10\Omega$.

$$\dot{\rho}_{cc} = -\gamma\rho_{cc} - i\frac{\Omega}{2}(\rho_{bc} - \rho_{cb}), \quad (9b)$$

$$\dot{\rho}_{bc} = -\gamma/2\rho_{bc} + i\frac{\Omega}{2}(\rho_{bb} - \rho_{cc}), \quad (9c)$$

$$\dot{\rho}_{aa} = \gamma\rho_{cc}. \quad (9d)$$

The coherent terms couple the populations ρ_{bb} and ρ_{cc} to the coherence ρ_{bc} and ρ_{cb} , but have no contribution to the dynamics of coherence $\rho_{bc} + \rho_{cb}$, because $\dot{\rho}_{bc} + \dot{\rho}_{cb} = -\gamma/2(\rho_{bc} + \rho_{cb})$, which is only exponentially damped dynamics with decay rate $\gamma/2$. This means that we can not characterize LEP by observe the dynamics of $(\rho_{bc} + \rho_{cb})$. Meanwhile, as shown in Eq. (9)(a), the damping term, proportional to γ , does not affect ρ_{bb} . It contributes to the decay of ρ_{cc} and to the corresponding increase of ρ_{aa} . The competition between the coherent coupling and the damping term of two states $\{|b\rangle, |c\rangle\}$ induce the third-order LEP (with the average decay rate $\gamma/2$), which is the phase transition point of passive \mathcal{PT} Hamiltonian [28]. And their contributions to $|a\rangle$ give rise the second-order LEP (with average decay rate $\gamma/4$ and half rotating frequency of the third-order LEP).

There are only three independent variables in Eqs. (9): $x = \rho_{bb}$, $y = \rho_{cc}$ and $z = -i(\rho_{bc} - \rho_{cb})$, which describe the dynamics of the subsystem $\{|b\rangle, |c\rangle\}$. With these new notations, we find the dynamics,

$$\begin{pmatrix} \dot{x} \\ \dot{y} \\ \dot{z} \end{pmatrix} = \begin{pmatrix} 0 & 0 & -\Omega/2 \\ 0 & -\gamma & \Omega/2 \\ \Omega & -\Omega & -\gamma/2 \end{pmatrix} \begin{pmatrix} x \\ y \\ z \end{pmatrix}. \quad (10)$$

Eigenvalues of the 3×3 matrix in Eq. (10) are $-(\gamma \mp \kappa)/2$ ($= \lambda_{5,6}$) and $-\gamma/2$ ($= \lambda_7$). The eigenvalues can be real or complex, leading to the two different regimes qualitatively analysed above and inducing the the third-order LEP at $\kappa = 0$. Besides that, we also derive their dynamical evolution analytically

$$x(t) = \frac{e^{-\frac{1}{2}\gamma t}}{\kappa^2} \left[(\gamma^2 - 2\Omega^2) \cosh\left(\frac{\kappa t}{2}\right) + \gamma\kappa \sinh\left(\frac{\kappa t}{2}\right) - 2\Omega^2 \right], \quad (11a)$$

$$y(t) = \frac{e^{-\frac{1}{2}\gamma t}}{\kappa^2} 4\Omega^2 \sinh^2\left(\frac{\kappa t}{4}\right), \quad (11b)$$

$$z(t) = \frac{e^{-\frac{1}{2}(\gamma+\kappa)t}}{\kappa^2} \Omega \left[\gamma \left(e^{\frac{\kappa t}{2}} - 1 \right)^2 + \kappa (e^{\kappa t} - 1) \right]. \quad (11c)$$

We show the dynamics of $x(t), y(t), z(t)$ in Fig. 3. When the decay rate is weak ($\gamma < 2\Omega$), the evolution is described by damped oscillation with decay rates $\gamma/2$ (subsystem) and $\gamma/4$ (full system), respectively. Obviously, increasing γ , the evolution approaching to the stationary state will become faster, which corresponds to the quantum anti-Zeno effect [51]. When the decay rate $\gamma > 2\Omega$, all the eigenvalues are real and the dynamics exhibits an irreversible damping. In the limit of strong decay, $\gamma \gg 2\Omega$, the relaxation time scale is determined by

$$(\gamma - \kappa)/2 \approx \Omega^2/\gamma \ll \gamma, \quad (12)$$

so that the system will experience the metastable process for a long time scale when the system appears stationary, before eventually relaxing to $\rho_{ss} = |a\rangle$. This means that the larger γ is, the slower the system relaxes, which is a manifestation of the quantum Zeno [48, 52–55]. Our results show that, for a dissipative system, quantum Zeno and anti-Zeno effects correspond to the dynamical phenomena with strong and weak dissipation strengths, respectively. The LEP is thus the boundary between the quantum Zeno and anti-Zeno regimes and bridges the two previously independent effects [56].

As we mentioned before, this dynamics also leads to an effective decay from the state $|b\rangle$ to state $|a\rangle$, with the effective decay rate

$$\gamma_{b \rightarrow a} \approx \Omega^2/\gamma. \quad (13)$$

The same result can be found in [39, 57] by employing perturbation theory and adiabatic elimination of states $|c\rangle$ for a weakly driven between $|b\rangle \leftrightarrow |c\rangle$. The above analysis shows that, our dissipative three-level model can be used to engineer decay processes between state $|b\rangle$ and $|a\rangle$ just by tuning the Rabi frequency Ω .

C. Engineering the relaxation dynamics

1. Control Liouvillian dynamics through the initial state

As we discussed in last subsection, there exist two timescales of the relaxation process depending on the space spanned by the initial state. If the initial state is an arbitrary state in space $\{|a\rangle, \{|b\rangle, |c\rangle\}$, the relaxation timescale approaching to the stationary state $|a\rangle$ is determined by $\lambda_1 = -(\gamma - \kappa)/4$, and the fastest dynamical relaxation happens at LEP ($\gamma = 2\Omega$) (see Fig. 4(a)). On the other hand, if the initial state $\rho_{in} \subseteq \{|b\rangle, |c\rangle\}$, as shown in Fig. 4(b), the relaxation timescale is determined by $\lambda_5 = -(\gamma - \kappa)/2$. This means that we can speed up relaxation in the convergence to stationarity by engineering the initial state, which is, the so-called Mpemba

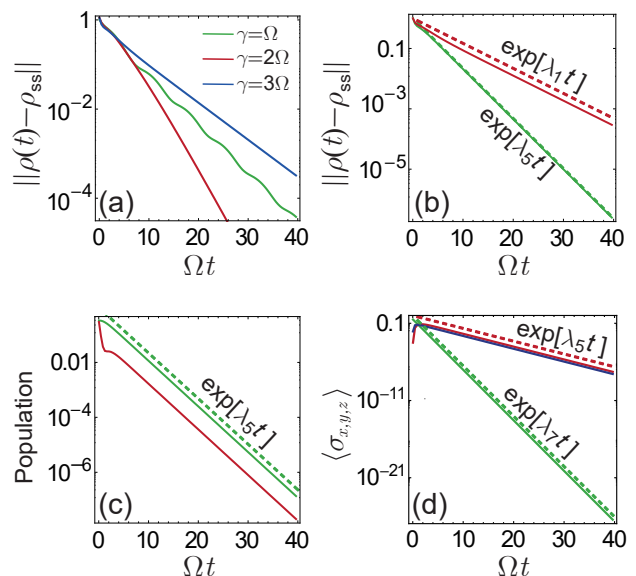


Figure 4. (a) Distance between the time-evolved state $\rho(t)$ and the stationary state $\rho_{ss} = |a\rangle$ for an initial random state in the full space with $\gamma = \Omega$ (Green line), $\gamma = 2\Omega$ (Red line), and $\gamma = 3\Omega$ (Blue line), respectively. In this original case, the approach to stationary is governed by the eigenvalue λ_1 , and LEP leads to an exponentially faster convergence to the steady state with the rate $g_{\text{LEP}} = \gamma/4 = \Omega/2$. (b) Distance between the time-evolved state $\rho(t)$ and the stationary state ρ_{ss} . We compare the case of an initial random state in the full space (Red line) with the time evolution ensuring the initial state in the subspace of $\{|b\rangle, |c\rangle\}$ (Green line). While in the original case, the approach to stationary is governed by the eigenvalue λ_1 (Red dashed line), the special set of initial state leads to an exponentially faster convergence to the steady state with the rate given by λ_5 (Green dashed line). (c) Population dynamics versus evolution time for an initial random state in the full space (Green line: $\text{Tr}[\rho(t)|b\rangle\langle b|]$, Red line: $\text{Tr}[\rho(t)|c\rangle\langle c|]$), and the time scale is governed by the eigenvalue λ_5 (Green dashed line). (d) Observable dynamics versus evolution time for an initial random state in the full space (Green line: $\langle \sigma_x \rangle = \text{Tr}[\rho(t)\sigma_x]$, Red line: $\langle \sigma_y \rangle = \text{Tr}[\rho(t)\sigma_y]$, Blue line: $\langle \sigma_z \rangle = \text{Tr}[\rho(t)\sigma_z]$), and the time scale are different: for σ_x it is governed by the eigenvalue λ_7 (Green dashed line) and for $\sigma_{y,z}$ they are governed by the eigenvalue λ_5 (Red dashed line). All the y axes are in logarithmic scale and the parameters for (b-d) are $\gamma/\Omega = 3$. We have to mention here that the real dynamics (Solid lines) and exponential decay function (Dashed lines) do not coincide at short times. This is because at short time, the decay rate is determined by all decay modes while at long time it decays with time exponentially.

effect [1, 2, 17]. We can understand this by looking the coefficients a_i of the initial state decomposition into the left eigenmatrices L_i . It can be shown that the coefficients of subspace $\{|b\rangle, |c\rangle\}$ decomposition into $L_{1\sim 4}$ are all vanished, i.e., $a_{1\sim 4} = \text{Tr}[L_{1\sim 4}\rho_{in}] = 0$ (see Appendix

A for further details). In this case

$$\rho(t) = \rho_{ss} + \sum_{i=5}^8 a_i e^{\lambda_i t} R_i, \quad (14)$$

therefore the asymptotic decay rate is $-\text{Re}[\lambda_5] = (\gamma - \kappa)/2$, which can get $g_{\text{LEP}} = \gamma/2$. In Fig. 4(b), we compare the timescales for different initial states. It presents that if the initial state is in the full space, the approach to the stationary state is governed by the eigenvalue λ_1 (Red dashed line), while the initial state in the subspace leads to an exponentially faster relaxation to the stationary state with the rate given by $\lambda_5 = -(\gamma - \kappa)/2$ (Green dashed line).

In addition to the dependence of the relaxation rate on the initial state, we also find that the observable values have significant effects on the relaxation rate (see Fig. 4(c,d)). For instance, because $\text{Tr}[|i\rangle\langle i|R_{1\sim 4}] = 0$ ($i = a, b, c$), the dynamics of the state populations approaching to stationarity is governed by the eigenvalue λ_5 (Fig. 4(c)). Moreover, the eigenmatrices $R_{5,6}$ describe the decay of $\sigma_{y,z}$ in the subspace $\{|b\rangle, |c\rangle\}$ with rates $\text{Re}[\lambda_{5,6}] = (\gamma \mp \kappa)/2$, while $R_8(\lambda_8)$ is associated with σ_x (see Appendix A for further details). Whereas there occurs only damped dynamics in the subspace spanned by operators σ_x , the oscillatory evolution at frequency $|\text{Im}[\lambda_5]|$ in the subspace spanned by vectors $\sigma_{y,z}$ allows to identify the third-order LEP [24, 31, 34]. Considering that the final state $\rho_{ss} = |a\rangle$ is independent on the parameters of the system, we can speed up the relaxation process by combining the acceleration effect of LEP and the initial state generation.

2. Tuning the Liouvillian gap through Floquet modulation

We find that the Liouvillian gap can be further increased under time-periodic (Floquet) dissipation with dissipation rate γ given by

$$\gamma(t) = \begin{cases} 0 & nT \leq t < nT + \tau, \\ \gamma & nT + \tau \leq t < (n+1)T. \end{cases} \quad (15)$$

Here $n \in \mathbb{Z}$, $T = 2\pi/\omega$ is the period of the Liouvillian i.e., $\mathcal{L}(t+T) = \mathcal{L}(t)$ with ω the modulation frequency, and τ is the off-duty time interval with no decay in each cycle. The density matrix at any time t is determined by the time-evolution operator $\mathcal{P}(t) = \mathbb{T} \exp(\int_0^t \mathcal{L}(t') dt')$, where \mathbb{T} is the time-ordering operator.

In analogy to the case of a non-Hermitian Hamiltonian system [54, 58], we can now formally define a Floquet generator for our case, an effective time-independent generator \mathcal{L}_F such that $\mathcal{P}(T) = \exp(\mathcal{L}_F T)$ [59–62]. Since the UD-OD transitions of the dynamics are determined by the degeneracies of the eigenvalues λ^P of the time-evolution operator \mathcal{P} , we adopt a dimensionless parameter $\mu = (|\lambda_+^P| - |\lambda_-^P|) / (|\lambda_+^P| + |\lambda_-^P|)$ to characterize the transition. Here, λ_{\pm}^P denote two eigenvalues with bifurcation structure, and $\mu = 0$ marks the two eigenvalues are

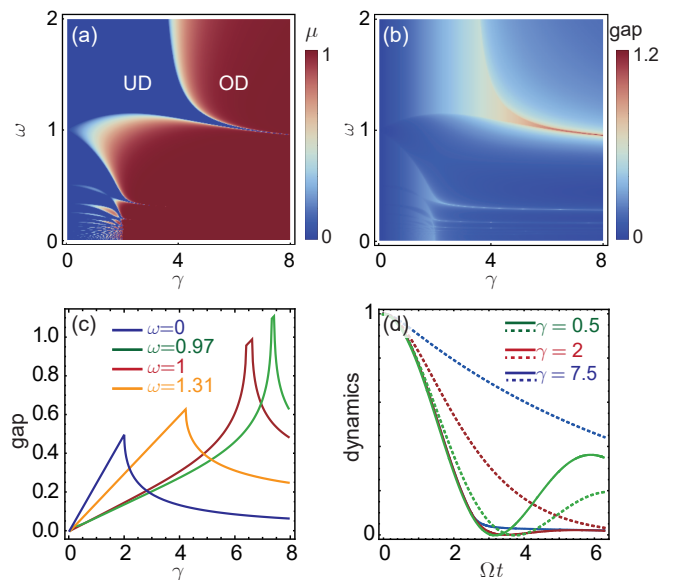


Figure 5. (a) Phase diagram in the $\omega - \gamma$ plane. Color contour shows the dimensionless parameter μ . Here we set $\Omega = 1, \tau = T/2.5$. Regions with vanishing μ correspond to the UD regime, while the colored regions correspond to the OD regime. (b) Liouvillian spectral gap as function of ω and γ . (c) Liouvillian spectral gap as a function of γ with $\omega = 0$ (Blue line), $\omega = 0.97$ (Green line), $\omega = 1$ (Red line) and $\omega = 1.31$ (Orange line), respectively. (d) The dynamics of the population of $|b\rangle$ with $\omega = 0$ (Dashed lines) and $\omega = \Omega$ (Solid lines). The other parameters are $\omega = 0.5$ (Green lines), 2 (Red lines) and 7.5 (Blue lines).

complex conjugate and the system is in the UD regime, while $\mu > 0$ are in the OD regime (see Fig. 5(a)). We can see the Floquet method enriches the phase diagram. In contrast with the static dissipation ($\omega = 0$), where the phase transition and LEPs appears at $\Omega/\gamma = 2$, phase transitions under time-periodic dissipation depends on the modulation frequency ω and can occur at vanishing small dissipation strength.

Beyond that, we are more interested in the effect of modulation on the energy gap. As shown in Fig. 5(b-c), Floquet method increase the gap and the maximal gap appears at the LEP which is a different point with the static case. In the case of static dissipation ($\omega = 0$), the $g_{\text{max}} = g_{\text{LEP}} = \Omega/2$ when $\gamma/\Omega = 2$. The gap under time-periodic dissipation depends on the modulation frequency ω and can even be significantly increased to bigger than Ω (see Fig. 5(c)). Fig. 5(d) plots the dynamics of the population of state $|b\rangle$. We compare the two different cases, $\omega = 0$ (dashed lines) and $\omega = \Omega$ (the solid lines). These results illustrate that the LEP gap can surpass its static limit through Floquet engineering and thus further accelerates the relaxation.

IV. APPLICATIONS IN GROUND STATE COOLING OF TRAPPED IONS

In the following, we demonstrate the power of this approach with a practical application, i.e., the ground state cooling of trapped ions. Through analytical and numerical analysis, we will illustrate that optimal cooling conditions in the sideband and EIT approaches can be obtained, which agree with existing experiments. Our LEP gap condition provides a new perspective on optimal cooling conditions and may simulate more studies for a wide range of quantum engineering applications.

A. Sideband cooling

As shown in Fig. 6, we consider laser-ion interactions in the Lamb-Dicke limit. Dynamics is governed by Hamiltonian

$$H = \nu a^\dagger a + \Delta |e\rangle\langle e| - \frac{1}{2}\Omega_g \sigma^x + \frac{1}{2}\Omega(a^\dagger + a)\sigma^y, \quad (16)$$

and jump operator $J = \sqrt{\gamma}|g\rangle\langle e|$. γ is the linewidth of the state $|e\rangle$, which is coupled to state $|g\rangle$ by a cooling laser field of frequency ω_l , Rabi frequency Ω_g , and detuning $\Delta = \omega_{ge} - \omega_l$, where ω_{ge} is the frequency of the bare atomic transition $|e\rangle \leftrightarrow |g\rangle$. ν is the trap frequency and $a(a^\dagger)$ is annihilation (creation) operator of phonons. $\Omega = \eta\Omega_g$ describes the effective coupling between the phonon and internal state and η is the Lamb-Dicke parameter. When $\Delta \simeq \nu$, the red sideband transition is nearly resonant, and the non-resonant transitions, i.e., the carrier transition and blue sideband transition, will induce the ac Stark shift to $|e\rangle(|g\rangle)$ by $\delta(-\delta)$, respectively. This is a good approximation that just considering shift caused by carrier transition, and under this approximation we get $\delta = (\sqrt{\Omega_g^2 + \Delta^2} - \Delta)/2$.

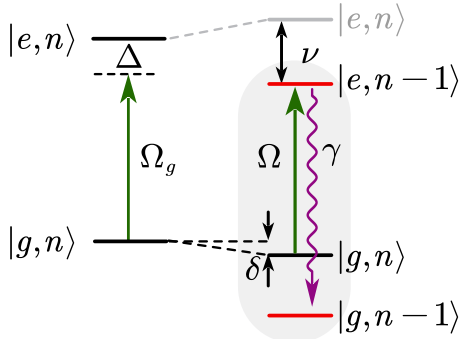


Figure 6. Schematic of the sideband cooling process. The cooling laser with frequency ω_l drives the transition $|e\rangle \leftrightarrow |g\rangle$ with Rabi frequency Ω_g and detuning $\Delta = \omega_{eg} - \omega_l$, which leads to the ac Stark shift δ . Ω is the effective coupling strength between the red sideband transition $|g\rangle|n\rangle \leftrightarrow |e\rangle|n-1\rangle$ with n the phonon number and η the Lamb-Dicke parameter.

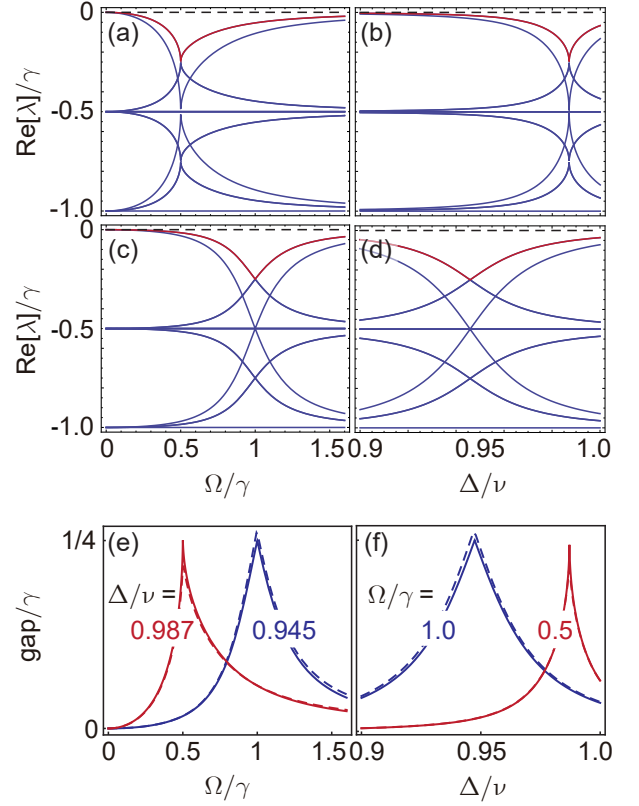


Figure 7. (a-d) Real parts of the Liouvillian spectra of the analytical results. The dashed lines are λ_0 and the red lines are λ_1 . The parameters are (a): $\Delta = 0.987\nu$, (b): $\Omega = 0.5\gamma$, (c): $\Delta = 0.945\nu$, and (d): $\Omega = \gamma$. (e-f) Gap as functions of Ω/γ (e) and Δ/ν (f). (e): $\Delta = 0.987\nu$ (Red lines) and $= 0.945\nu$ (Blue lines), (f): $\Omega = \Omega_g\eta = 0.5\gamma$ (Red lines) and $= \gamma$ (Blue lines), respectively. The solid lines correspond to the analytical results from eq. (17) and the dashed lines are the results from the full Liouvillian. The other parameters are $\eta = 0.1, \nu = 1, \gamma = 0.032$.

In order to obtain the optimal cooling condition, we reduce the overall dynamics to a low-dimensional subsystem $\{|g\rangle|1\rangle, |g\rangle|0\rangle, |e\rangle|1\rangle, |e\rangle|0\rangle\}$ to obtain analytical results (see Appendix B for details). It is very helpful for us to understand the whole cooling process. Based on the perturbative calculations for this finite systems, we get that $\lambda_{1(3)} = -(\gamma \mp \kappa')/4 + i(\Delta + 2\delta + \nu)/2$ and the gap

$$g = \text{Re}\left[\frac{1}{4}(\gamma - \kappa')\right], \quad (17)$$

with $\kappa' = \sqrt{(\gamma - 2i(\Delta + 2\delta - \nu))^2 - 4\Omega^2}$. In Fig. 7 (a-d), we plot the analytical results of the spectra. It is obvious that the LEPs can only occur under the condition $\Delta + 2\delta - \nu = 0$. With $\delta = (\sqrt{\Omega_g^2 + \Delta^2} - \Delta)/2$, we obtain the condition to generate LEP,

$$\Omega^2 + \Delta^2 = \nu^2. \quad (18)$$

Under this condition, the eigenvalues $\lambda_{1(3)}$ become

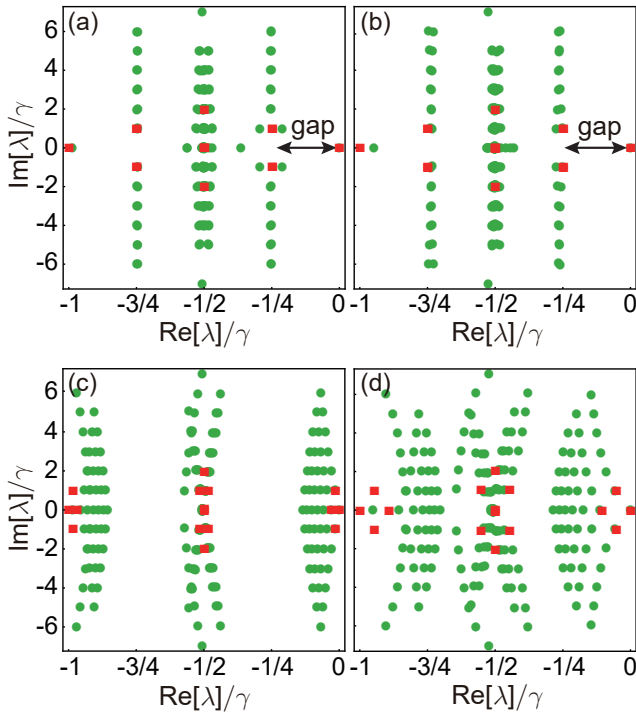


Figure 8. Spectral properties of the Liouvillian. (a-b) in the LEP condition ($\Omega^2 + \Delta = \nu^2$), and the parameters of ($\Omega/\gamma, \Delta/\nu$) are (a): (0.5, 0.987), (b): (1, 0.945), respectively. Fig. (c-d) not in the LEP condition ($\Omega^2 + \Delta \neq \nu^2$), the parameters of ($\Omega/\gamma, \Delta/\nu$) are (c): (1, 0.987), (d): (0.2, 1). The green dots are the results from the full Liouvillian and the red squares are the eigenvalues of the analytical results. The other parameters are the same with Fig. 7.

$\lambda_{1(3)} = -(\gamma \mp \kappa)/4 + i\nu$, whose real parts are the same with three-level dissipative system shown in Fig. 2(b) and the imaginary parts connote rotating. The physical mechanism underlying condition (18) is that the detuning Δ needs to be adjusted according to the ac Stark shift of the atomic levels to ensure that the red sideband transition is exactly on resonance. Under this premise, the level structure shown in Fig. 6 can be considered as a simple three-level dissipative system discussed in section III. When $\Omega \geq \gamma/2$, $\text{Re}[\lambda_1] = \text{Re}[\lambda_3] = -\gamma/4$, and we get the maximum value $g_{\max} = \gamma/4$. Particularly, when $\Omega = \gamma/2$, $\kappa = \sqrt{\gamma^2 - 4\Omega^2} = 0$, $\lambda_1 = \lambda_3$ and $R_1 = R_3$ (see Appendix B), LEP occurs.

In Fig.7 (e-f), we compare the gap given by Eq. (17) (the solid lines) with the numerical results calculated from the full master equation (the dashed lines). Although our analytical results about spectrum and gap are obtained from the subsystem of the sideband cooling, they match very well with the numerical results calculated from the full-system. As shown in Fig. 8, the real parts of the eigenvalues $\lambda_{i \geq 1}$, which give the relaxation rates of all the decay modes of the system, mainly can be divided into several characteristic intervals. It approximately could be $\{-\gamma/4, -\gamma/2, -3\gamma/4, -\gamma\}$ under

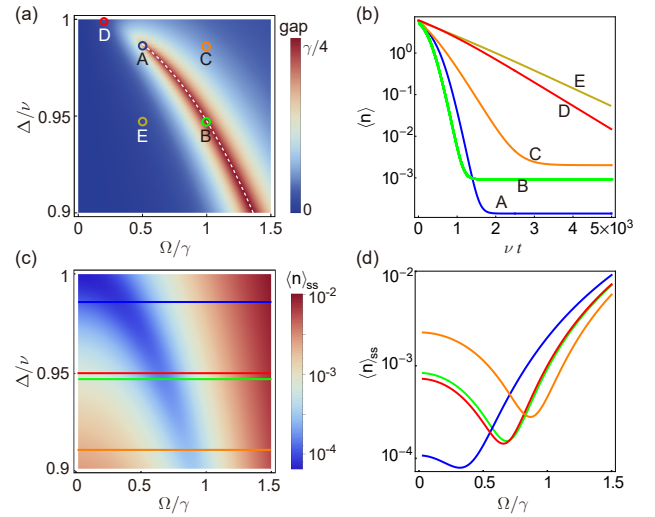


Figure 9. (a) Gap properties of the full Liouvillian. The white dashed line corresponds to $\Omega^2 + \Delta^2 = \nu^2$. The parameters ($\Omega/\gamma, \Delta/\nu$) are (0.5, 0.987)(A), (1, 0.945)(B), (1, 0.987)(C), (0.2, 1)(D), (0.5, 0.945)(E) and $g_A = g_B > g_C > g_D > g_E$. (b) The average phonon number $\langle n \rangle$ as a function of time calculated with full master equation with the parameters of A, B, C, D, E, respectively. (c) Cooling limit $\langle n \rangle_{ss}$ as functions of detuning Δ/ν and effective Rabi frequency of red sideband transition Ω/γ . (d) $\langle n \rangle_{ss}$ as a function of effective Rabi frequency of red sideband transition Ω/γ with $\Delta/\nu = 0.987$ (Blue line), 0.95 (Red line), 0.945 (Green line) and 0.91 (Orange). The other parameters are the same with Fig. 7.

the condition (18) (see Fig. 8 (a-b)), otherwise, it becomes to be $\{0, -\gamma/2, -\gamma\}$ when $\Omega/\gamma > 1/2$ (see Fig. 8 (c)). As shown in Fig. 8 (c-d), different with the 3-level dissipation system, it features a so-called metastable regime either $\Omega/\gamma > 1/2$ or $\Omega/\gamma < 1/2$, which occurs when low lying eigenvalues become separated from the rest of the spectrum [14]. The imaginary parts of the eigenvalues, which give the rotating rates of the decay modes approximately equal to $\text{Im}[\lambda_{i \geq 1}] \approx (\Delta + 2\delta + n\nu)/2$ are mainly determined by phonon energy.

In Fig. 9(a), we plot the gap g as functions of Ω/γ and Δ/ν by using the full master equation. The point A corresponds to the LEP, and the dashed white line is the condition of $g = g_{\max}$ that combines red sideband transition resonant condition in Eq. (18) as we discussed before. The numerical results and the analytical results are matched very well. Fig. 9(b) shows the the dynamics of the full system for some set of parameters (the points A, B, C, D in Fig. 9(a)). It indicates that the gap g provides a good description of the cooling time. And at the LEP, the system not only reaches stationary state at a significantly faster pace, but also obtains a lower phonon number (see Fig. 9(c-d)). Therefore, we believe that the best cooling effect can be obtained by the system parameters at the LEP.

B. EIT cooling

For the EIT cooling method discussed in [5, 7, 9], we find that the optimal parameter selection could be explained by the gap at LEP. As shown in Fig.10 (a), the detuned laser of frequency ω_r and Rabi frequency Ω_r , couples the transition $|r\rangle \leftrightarrow |e\rangle$ with detuning $\Delta_r = \omega_r - \omega_{er}$. It leads to two dressed states $|+\rangle$ and $|-\rangle$ shown in Fig.10 (b) with energy $\omega_+ = \Delta_r + \delta_r, \omega_- = -\delta_r$ [5, 63], respectively. Here, $\delta_r = (\sqrt{\Omega_r^2 + \Delta_r^2} - |\Delta_r|)/2$ is the ac Stark shift induced by the coupling laser Ω_r .

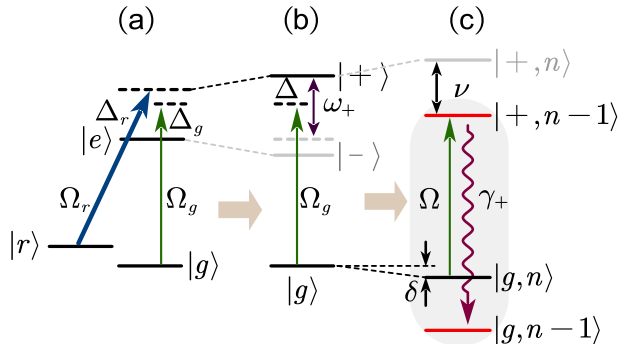


Figure 10. (a) Levels and transitions of the EIT cooling scheme (found in many species used for ion trapping). (b) The dressed levels what the cooling laser Ω_g couples. (c) When the cooling laser is near resonant with the red sideband transition of the dressed state $|+\rangle$, then this EIT cooling model can be equivalent to the model we discussed in example II.

If we turn the detuning frequency Δ_g of Ω_g closing to Δ_r , then $|+\rangle = \sin \phi |e\rangle + \cos \phi |r\rangle$ ($\tan \phi = \Omega_r / (\sqrt{\Omega_r^2 + \Delta_r^2} + \Delta_r)$) is chosen to replace $|e\rangle$ in the sideband cooling model (see Fig.10 (c)). Here we just replace

$$\gamma \rightarrow \gamma_+ = \gamma_e \sin^2 \phi = \frac{\gamma_e}{2} \left(1 - \frac{\Delta_r}{\sqrt{\Omega_r^2 + \Delta_r^2}}\right), \quad (19)$$

$$\Omega \rightarrow \eta \sin \phi \Omega_g, \quad (20)$$

$$\Delta \rightarrow \omega_+ - \Delta_g. \quad (21)$$

Then the optimal condition of g_{\max} shown in Eq. (18) will become to

$$\frac{\eta^2}{2} \left(1 - \frac{\Delta_r}{\sqrt{\Omega_r^2 + \Delta_r^2}}\right) \Omega_g^2 + \left(\frac{\sqrt{\Omega_r^2 + \Delta_r^2} + \Delta_r}{2} - \Delta_g\right)^2 = \nu^2.$$

Appendix A: Liouvillian spectrum of a dissipative three-level system

We consider a simple dissipative three-level system of Fig. 2(b), and the dynamics is described by a Lindblad master equation

$$\mathcal{L}\rho = -i[H, \rho] + J\rho J^\dagger - \frac{1}{2}\{J^\dagger J, \rho\}, \quad (A1)$$

If we ignore the higher order terms $\mathcal{O}(\eta^2)$, Eq. (22) can be rewritten as

$$\frac{\sqrt{\Omega_r^2 + \Delta_r^2} + \Delta_r}{2} - \Delta_g = \delta_r + \Delta_r - \Delta_g = \nu. \quad (23)$$

It is in accordance with the generalized cooling condition given in experiment works of Ref. [7, 9], thus our LEP method offers a fresh understanding of optical cooling condition.

V. DISCUSSION

In summary, we have studied how to engineer relaxation dynamics of Markovian open quantum systems with an arbitrary initial state. Our results have shown, for an arbitrary initial state, a speed-up relaxation can be achieved by setting the parameters of the system at LEP, where the slowest decay mode degenerates with a faster decay mode. In addition, our LEP-based accelerated approach can also be applied to accelerate the relaxation to stationarity in Floquet dissipative quantum dynamics. We have shown the relaxation processes can be dramatically faster than the static case by periodically modulating the dissipation strength. Finally, We have demonstrated the applications of our method for speeding up cooling processes in ground state cooling of trapped ions. In a broader view, our ideas may be still instructive for optimal parameter options to accelerate the cooling process even for simultaneous cooling of multiple phonon modes in a ion crystal. Therefore, our method would be in general and would facilitate the optical parameters setting in the experiments with open quantum many-body systems. Together with well-developed techniques of engineering quantum states, our work provides a powerful tool for exploring and utilizing true quantum LEP effects as examples of engineered relaxation dynamics [64].

ACKNOWLEDGMENTS

This work was supported by the National Nature Science Foundation of China (Grants No. 12174448, 12074433, 12004430), the Innovation Program for Quantum Science and Technology (2021ZD0301601) and the Science and Technology Innovation Program of Hunan Province (2022RC1194, 2023JJ10052).

with the Hamiltonian $H = \Omega/2(|c\rangle\langle b| + |b\rangle\langle c|)$ and a jump operator $J = \sqrt{\gamma}|a\rangle\langle c|$.

To study the Liouvillian spectra and LEPs, we first represent the Liouvillian superoperator \mathcal{L} in a matrix form by recasting the above master equation as a matrix differential equation for the vectorized state of the density operator ρ . With the definitions that $|a\rangle = (1, 0, 0)^T$, $|b\rangle = (0, 1, 0)^T$, $|c\rangle = (0, 0, 1)^T$, the Liouvillian superoperator is given by

$$\mathcal{L} = \begin{pmatrix} 0 & 0 & 0 & 0 & 0 & 0 & 0 & 0 & \gamma \\ 0 & 0 & \frac{i\Omega}{2} & 0 & 0 & 0 & 0 & 0 & 0 \\ 0 & \frac{i\Omega}{2} & -\frac{\gamma}{2} & 0 & 0 & 0 & 0 & 0 & 0 \\ 0 & 0 & 0 & 0 & 0 & 0 & -\frac{i\Omega}{2} & 0 & 0 \\ 0 & 0 & 0 & 0 & 0 & \frac{i\Omega}{2} & 0 & -\frac{i\Omega}{2} & 0 \\ 0 & 0 & 0 & 0 & \frac{i\Omega}{2} & -\frac{\gamma}{2} & 0 & 0 & -\frac{i\Omega}{2} \\ 0 & 0 & 0 & -\frac{i\Omega}{2} & 0 & 0 & -\frac{\gamma}{2} & 0 & 0 \\ 0 & 0 & 0 & 0 & -\frac{i\Omega}{2} & 0 & 0 & -\frac{\gamma}{2} & \frac{i\Omega}{2} \\ 0 & 0 & 0 & 0 & 0 & -\frac{i\Omega}{2} & 0 & \frac{i\Omega}{2} & -\gamma \end{pmatrix} \quad (\text{A2})$$

The eigenvalues of \mathcal{L} are

$$\lambda_0 = 0, \lambda_{1(2)} = -\frac{1}{4}(\gamma - \kappa), \lambda_{3(4)} = -\frac{1}{4}(\gamma + \kappa), \lambda_{5,6} = -\frac{1}{2}(\gamma \mp \kappa), \lambda_{7(8)} = -\frac{\gamma}{2}. \quad (\text{A3})$$

with $\kappa = \sqrt{\gamma^2 - 4\Omega^2}$. Both the right and left eigenmatrices of the Liouvillian superoperators can be constructed to be Hermitian, they are

$$\begin{aligned} R_0 = \rho_{ss} &= \begin{pmatrix} 1 & 0 & 0 \\ 0 & 0 & 0 \\ 0 & 0 & 0 \end{pmatrix}, & R_1 &\propto \begin{pmatrix} 0 & -\frac{i(\gamma+\kappa)}{2\Omega} & 1 \\ \frac{i(\gamma+\kappa)}{2\Omega} & 0 & 0 \\ 1 & 0 & 0 \end{pmatrix}, & R_2 &\propto \begin{pmatrix} 0 & \frac{(\gamma+\kappa)}{2\Omega} & i \\ \frac{(\gamma+\kappa)}{2\Omega} & 0 & 0 \\ -i & 0 & 0 \end{pmatrix}, \\ R_3 &\propto \begin{pmatrix} 0 & -\frac{i(\gamma-\kappa)}{2\Omega} & 1 \\ \frac{i(\gamma-\kappa)}{2\Omega} & 0 & 0 \\ 1 & 0 & 0 \end{pmatrix}, & R_4 &\propto \begin{pmatrix} 0 & \frac{(\gamma-\kappa)}{2\Omega} & i \\ \frac{(\gamma-\kappa)}{2\Omega} & 0 & 0 \\ -i & 0 & 0 \end{pmatrix}, & R_5 &\propto \begin{pmatrix} -\frac{2\gamma}{\gamma-\kappa} & 0 & 0 \\ 0 & \frac{2\gamma}{\gamma-\kappa} - 1 & \frac{i(\gamma+\kappa)}{2\Omega} \\ 0 & -\frac{i(\gamma+\kappa)}{2\Omega} & 1 \end{pmatrix}, \\ R_6 &\propto \begin{pmatrix} -\frac{2\gamma}{\gamma+\kappa} & 0 & 0 \\ 0 & \frac{2\gamma}{\gamma+\kappa} - 1 & \frac{i(\gamma-\kappa)}{2\Omega} \\ 0 & -\frac{i(\gamma-\kappa)}{2\Omega} & 1 \end{pmatrix}, & R_7 &\propto \begin{pmatrix} -2 & 0 & 0 \\ 0 & 1 & \frac{i\gamma}{2\Omega} \\ 0 & -\frac{i\gamma}{2\Omega} & 1 \end{pmatrix}, & R_8 &\propto \begin{pmatrix} 0 & 0 & 0 \\ 0 & 0 & 1 \\ 0 & 1 & 0 \end{pmatrix}, \end{aligned} \quad (\text{A4})$$

$$\begin{aligned} L_0 &= \begin{pmatrix} 1 & 0 & 0 \\ 0 & 1 & 0 \\ 0 & 0 & 1 \end{pmatrix}, & L_1 &\propto \begin{pmatrix} 0 & \frac{i(\gamma+\kappa)}{2\Omega} & 1 \\ -\frac{i(\gamma+\kappa)}{2\Omega} & 0 & 0 \\ 1 & 0 & 0 \end{pmatrix}, & L_2 &\propto \begin{pmatrix} 0 & \frac{(\gamma+\kappa)}{2\Omega} & -i \\ \frac{(\gamma+\kappa)}{2\Omega} & 0 & 0 \\ i & 0 & 0 \end{pmatrix}, \\ L_3 &\propto \begin{pmatrix} 0 & \frac{i(\gamma-\kappa)}{2\Omega} & 1 \\ -\frac{i(\gamma-\kappa)}{2\Omega} & 0 & 0 \\ 1 & 0 & 0 \end{pmatrix}, & L_4 &\propto \begin{pmatrix} 0 & \frac{(\gamma-\kappa)}{2\Omega} & -i \\ \frac{(\gamma-\kappa)}{2\Omega} & 0 & 0 \\ i & 0 & 0 \end{pmatrix}, & L_5 &\propto \begin{pmatrix} 0 & 0 & 0 \\ 0 & \frac{2\gamma}{\gamma-\kappa} - 1 & -\frac{i(\gamma+\kappa)}{2\Omega} \\ 0 & \frac{i(\gamma+\kappa)}{2\Omega} & 1 \end{pmatrix}, \\ L_6 &\propto \begin{pmatrix} 0 & 0 & 0 \\ 0 & \frac{2\gamma}{\gamma+\kappa} - 1 & -\frac{i(\gamma-\kappa)}{2\Omega} \\ 0 & \frac{i(\gamma-\kappa)}{2\Omega} & 1 \end{pmatrix}, & L_7 &\propto \begin{pmatrix} 0 & 0 & 0 \\ 0 & 1 & -\frac{i\gamma}{2\Omega} \\ 0 & \frac{i\gamma}{2\Omega} & 1 \end{pmatrix}, & L_8 &\propto \begin{pmatrix} 0 & 0 & 0 \\ 0 & 0 & 1 \\ 0 & 1 & 0 \end{pmatrix}. \end{aligned} \quad (\text{A5})$$

If the initial state is in this subspace $\{|b\rangle, |c\rangle\}$, it is easily get that $a_{1\sim 4} = \text{Tr}[L_{1\sim 4}\rho_{in}] = 0$. It means that the coefficients of subspace $\{|b\rangle, |c\rangle\}$ decomposition into $L_{1\sim 4}$ are all vanished.

Appendix B: Liouvillian spectrum of the subsystem of ground state cooling process

For the subsystem $\{|e\rangle|1\rangle, |e\rangle|0\rangle, |g\rangle|1\rangle, |g\rangle|0\rangle\}$, we calculate the spectrum of its superoperator \mathcal{L} and get

$$\begin{aligned} \lambda_0 &= 0, & \lambda_1 = \lambda_2^* &= -\frac{\gamma - \kappa'}{4} + i\frac{\alpha}{2}, & \lambda_3 = \lambda_4^* &= -\frac{\gamma + \kappa'}{4} + i\frac{\alpha}{2}, \\ \lambda_5 = \lambda_6^* &= -\frac{\gamma}{2} + i\alpha, & \lambda_{7(8)} &= -\frac{2\gamma \mp \epsilon}{4}, & \lambda_{9(10)} &= -\frac{2\gamma \mp \epsilon'}{4}, \end{aligned}$$

$$\lambda_{11} = \lambda_{12}^* = -\frac{3\gamma - \kappa'}{4} - i\frac{\alpha}{2}, \quad \lambda_{13} = \lambda_{14}^* = -\frac{3\gamma + \kappa'}{4} - i\frac{\alpha}{2}, \quad \lambda_{15} = -\gamma, \quad (\text{B1})$$

with

$$\kappa' = \sqrt{(\gamma + 2i\beta)^2 - 4\Omega^2}, \quad (\text{B2})$$

$$\alpha = \Delta + 2\delta + \nu, \quad (\text{B3})$$

$$\epsilon = \sqrt{-2\sqrt{(4(\beta^2 + \Omega^2) + \gamma^2)^2 - 16\gamma^2\Omega^2} - 8\beta^2 + 2\gamma^2 - 8\Omega^2}, \quad (\text{B4})$$

$$\epsilon' = \sqrt{2\sqrt{(4(\beta^2 + \Omega^2) + \gamma^2)^2 - 16\gamma^2\Omega^2} - 8\beta^2 + 2\gamma^2 - 8\Omega^2}, \quad (\text{B5})$$

where $\beta = 2\delta + \Delta - \nu$. The corresponding eigenmatrices are

$$R_0 = \begin{pmatrix} 0 & 0 & 0 & 0 \\ 0 & 0 & 0 & 0 \\ 0 & 0 & 0 & 0 \\ 0 & 0 & 0 & 1 \end{pmatrix},$$

$$R_1 \propto \begin{pmatrix} 0 & 0 & 0 & 0 \\ 0 & 0 & 0 & \frac{2\Omega}{2i\beta + \gamma + \kappa'^*} \\ 0 & 0 & 0 & 1 \\ 0 & \frac{2\Omega}{-2i\beta - \gamma + \kappa'} & 1 & 0 \end{pmatrix},$$

$$R_3 \propto \begin{pmatrix} 0 & 0 & 0 & 0 \\ 0 & 0 & 0 & -\frac{2\Omega}{-2i\beta - \gamma + \kappa'^*} \\ 0 & 0 & 0 & 1 \\ 0 & -\frac{2\Omega}{2i\beta - \gamma + \kappa'} & 1 & 0 \end{pmatrix},$$

$$R_5 \propto \begin{pmatrix} 0 & 0 & 0 & 1 \\ 0 & 0 & 0 & 0 \\ 0 & 0 & 0 & 0 \\ 1 & 0 & 0 & 0 \end{pmatrix},$$

$$R_7 \propto \begin{pmatrix} 0 & 0 & 0 & 0 \\ 0 & -\frac{2\gamma - \epsilon}{4\gamma} & -\frac{\epsilon\Omega}{\gamma(4i\beta + \epsilon)} & 0 \\ 0 & -\frac{\epsilon\Omega}{\gamma(-4i\beta)} & -\frac{2\gamma + \epsilon}{4\gamma} & 0 \\ 0 & 0 & 0 & 1 \end{pmatrix},$$

$$R_9 \propto \begin{pmatrix} 0 & 0 & 0 & 0 \\ 0 & -\frac{2\gamma - \epsilon'}{4\gamma} & -\frac{\epsilon'\Omega}{\gamma(4i\beta + \epsilon')} & 0 \\ 0 & -\frac{\epsilon'\Omega}{\gamma(\epsilon' - 4i\beta)} & -\frac{2\gamma + \epsilon'}{4\gamma} & 0 \\ 0 & 0 & 0 & 1 \end{pmatrix},$$

$$R_{11} \propto \begin{pmatrix} 0 & -1 & -\frac{-2i\beta + \gamma + \kappa'}{2\Omega} & 0 \\ -1 & 0 & 0 & \frac{2\Omega}{2i\beta - \gamma + \kappa'} \\ -\frac{2i\beta + \gamma + \kappa'^*}{2\eta\Omega_g} & 0 & 0 & 1 \\ 0 & \frac{2\Omega}{-2i\beta - \gamma + \kappa'^*} & 1 & 0 \end{pmatrix},$$

$$R_{12} \propto \begin{pmatrix} 0 & -i & -\frac{i(-2i\beta + \gamma + \kappa')}{2\Omega} & 0 \\ i & 0 & 0 & \frac{2i\Omega}{2i\beta - \gamma + \kappa'} \\ \frac{i(2i\beta + \gamma + \kappa'^*)}{2\Omega} & 0 & 0 & i \\ 0 & -\frac{2i\Omega}{-2i\beta - \gamma + \kappa'^*} & -i & 0 \end{pmatrix},$$

$$R_{13} \propto \begin{pmatrix} 0 & -1 & -\frac{-2i\beta + \gamma - \kappa'}{2\Omega} & 0 \\ -1 & 0 & 0 & \frac{2\Omega}{2i\beta - \gamma - \kappa'} \\ -\frac{2i\beta + \gamma - \kappa'^*}{2\eta\Omega_g} & 0 & 0 & 1 \\ 0 & \frac{2\Omega}{-2i\beta - \gamma - \kappa'^*} & 1 & 0 \end{pmatrix},$$

$$R_2 \propto \begin{pmatrix} 0 & 0 & 0 & 0 \\ 0 & 0 & 0 & -\frac{2i\Omega}{2i\beta + \gamma + \kappa'^*} \\ 0 & 0 & 0 & -i \\ 0 & \frac{2i\Omega}{-2i\beta - \gamma + \kappa'} & i & 0 \end{pmatrix},$$

$$R_4 \propto \begin{pmatrix} 0 & 0 & 0 & 0 \\ 0 & 0 & 0 & \frac{2i\Omega}{-2i\beta - \gamma + \kappa'^*} \\ 0 & 0 & 0 & -i \\ 0 & -\frac{2i\Omega}{2i\beta - \gamma + \kappa'} & i & 0 \end{pmatrix},$$

$$R_6 \propto \begin{pmatrix} 0 & 0 & 0 & -i \\ 0 & 0 & 0 & 0 \\ 0 & 0 & 0 & 0 \\ i & 0 & 0 & 0 \end{pmatrix},$$

$$R_8 \propto \begin{pmatrix} 0 & 0 & 0 & 0 \\ 0 & -\frac{2\gamma + \epsilon}{4\gamma} & \frac{\epsilon\Omega}{\gamma(4i\beta - \epsilon)} & 0 \\ 0 & \frac{\epsilon\Omega}{\gamma(-4i\beta - \epsilon)} & -\frac{2\gamma - \epsilon}{4\gamma} & 0 \\ 0 & 0 & 0 & 1 \end{pmatrix},$$

$$R_{10} \propto \begin{pmatrix} 0 & 0 & 0 & 0 \\ 0 & -\frac{2\gamma + \epsilon'}{4\gamma} & \frac{\epsilon'\Omega}{\gamma(-\epsilon' + 4i\beta)} & 0 \\ 0 & \frac{\epsilon'\Omega}{\gamma(-\epsilon' - 4i\beta)} & -\frac{2\gamma - \epsilon'}{4\gamma} & 0 \\ 0 & 0 & 0 & 1 \end{pmatrix},$$

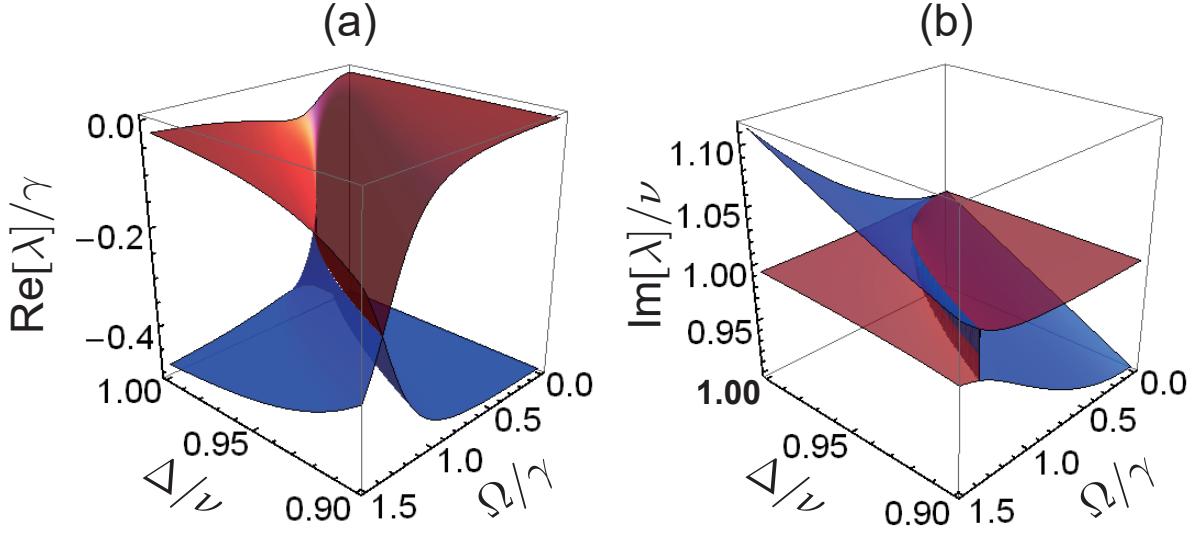


Figure B.1. (a) Real and (b) imaginary parts of λ_2 (red) and λ_4 (blue).

$$R_{14} \propto \begin{pmatrix} 0 & -i & -\frac{i(-2i\beta+\gamma-\kappa')}{2\Omega} & 0 \\ i & 0 & 0 & \frac{2i\Omega}{2i\beta-\gamma-\kappa'} \\ \frac{i(2i\beta+\gamma-\kappa'^*)}{2\Omega} & 0 & 0 & i \\ 0 & -\frac{2i\Omega}{-2i\beta-\gamma-\kappa'^*} & -i & 0 \end{pmatrix},$$

$$R_{15} \propto \begin{pmatrix} 1 & 0 & 0 & 0 \\ 0 & -1 & 0 & 0 \\ 0 & 0 & -1 & 0 \\ 0 & 0 & 0 & 1 \end{pmatrix}.$$

We are interested with the low lying eigenvalues, especially λ_1 which determines the spectral gap $g = \frac{1}{4}(\gamma - \kappa')$. We can see that when $\beta = 2\delta + \Delta - \nu = 0$ and $\gamma = 2\Omega$, we get $\kappa' = 0$ and $\lambda_{1(2)} = \lambda_{3(4)}$, $\lambda_{11(12)} = \lambda_{13(14)}$ (see Fig. B.1). As a result, we can find sets of simultaneous second-order LEP.

-
- [1] Federico Carollo, Antonio Lasanta, and Igor Lesanovsky, “Exponentially accelerated approach to stationarity in markovian open quantum systems through the mpemba effect,” *Phys. Rev. Lett.* **127**, 060401 (2021).
 - [2] Simon Kochsiek, Federico Carollo, and Igor Lesanovsky, “Accelerating the approach of dissipative quantum spin systems towards stationarity through global spin rotations,” *Phys. Rev. A* **106**, 012207 (2022).
 - [3] Tan Van Vu and Yoshihiko Hasegawa, “Toward relaxation asymmetry: Heating is faster than cooling,” *Physical Review Research* **3**, 043160 (2021).
 - [4] Alessio Lapolla and Aljaž Godec, “Faster Uphill Relaxation in Thermodynamically Equidistant Temperature Quenches,” *Physical Review Letters* **125**, 110602 (2020).
 - [5] Giovanna Morigi, Jürgen Eschner, and Christoph H. Keitel, “Ground state laser cooling using electromagnetically induced transparency,” *Phys. Rev. Lett.* **85**, 4458–4461 (2000).
 - [6] L. Feng, W. L. Tan, A. De, A. Menon, A. Chu, G. Pagano, and C. Monroe, “Efficient Ground-State Cooling of Large Trapped-Ion Chains with an Electromagnetically-Induced-Transparency Tripod Scheme,” *Physical Review Letters* **125**, 053001 (2020).
 - [7] Mu Qiao, Ye Wang, Zhengyang Cai, Botao Du, Pengfei Wang, Chunyang Luan, Wentao Chen, Heung-ryoul Noh, and Kihwan Kim, “Double-Electromagnetically-Induced-Transparency Ground-State Cooling of Stationary Two-Dimensional Ion Crystals,” *Physical Review Letters* **126**, 23604 (2021).
 - [8] Shuo Zhang, Jian-Qi Zhang, Wei Wu, Wan-Su Bao, and Chu Guo, “Fast cooling of trapped ion in strong sideband coupling regime,” *New Journal of Physics* **23**, 023018 (2021).
 - [9] Jie Zhang, Man-Chao Zhang, Yi Xie, Chun-Wang Wu, Bao-Quan Ou, Ting Chen, Wan-Su Bao, Paul Haljan, Wei Wu, Shuo Zhang, and Ping-Xing Chen, “Parallel

- electromagnetically induced transparency near ground-state cooling of a trapped-ion crystal,” *Phys. Rev. Applied* **18**, 014022 (2022).
- [10] Jens Honer, R. Löw, Hendrik Weimer, Tilman Pfau, and Hans Peter Büchler, “Artificial atoms can do more than atoms: Deterministic single photon subtraction from arbitrary light fields,” *Physical Review Letters* **107**, 093601 (2011).
- [11] C. Tresp, C. Zimmer, I. Mirgorodskiy, H. Gorniaczyk, A. Paris-Mandoki, and S. Hofferberth, “Single-photon absorber based on strongly interacting rydberg atoms,” *Phys. Rev. Lett.* **117**, 223001 (2016).
- [12] Asaf Paris-Mandoki, Christoph Braun, Jan Kumlin, Christoph Tresp, Ivan Mirgorodskiy, Florian Christaller, Hans Peter Büchler, and Sebastian Hofferberth, “Free-space quantum electrodynamics with a single rydberg superatom,” *Phys. Rev. X* **7**, 041010 (2017).
- [13] Nina Stiesdal, Hannes Busche, Jan Kumlin, Kevin Kleinbeck, Hans Peter Büchler, and Sebastian Hofferberth, “Observation of collective decay dynamics of a single rydberg superatom,” *Phys. Rev. Research* **2**, 043339 (2020).
- [14] Katarzyna Macieszczak, Mădălin Guță, Igor Lesanovsky, and Juan P. Garrahan, “Towards a theory of metastability in open quantum dynamics,” *Phys. Rev. Lett.* **116**, 240404 (2016).
- [15] Marko Znidarič, “Relaxation times of dissipative many-body quantum systems,” *Physical Review E* **92**, 042143 (2015).
- [16] Taiki Haga, Masaya Nakagawa, Ryusuke Hamazaki, and Masahito Ueda, “Liouvillian Skin Effect: Slowing down of Relaxation Processes without Gap Closing,” *Physical Review Letters* **127**, 70402 (2021).
- [17] E B Mpemba and D G Osborne, “Cool?” *Physics Education* **4**, 172–175 (1969).
- [18] Zhiyue Lu and Oren Raz, “Nonequilibrium thermodynamics of the Markovian Mpemba effect and its inverse,” *Proc. Natl Acad. Sci. USA* **114**, 5083–5088 (2017).
- [19] Israel Klich, Oren Raz, Ori Hirschberg, and Marija Vucelja, “Mpemba Index and Anomalous Relaxation,” *Physical Review X* **9**, 21060 (2019), 1711.05829.
- [20] Avinash Kumar and John Bechhoefer, “Exponentially faster cooling in a colloidal system,” *Nature* **584**, 64–68 (2020), 2008.02373.
- [21] W D Heiss, “Exceptional points of non-Hermitian operators,” *Journal of Physics A: Mathematical and General* **37**, 2455 (2004).
- [22] Emil J. Bergholtz, Jan Carl Budich, and Flore K. Kunst, “Exceptional topology of non-Hermitian systems,” *Reviews of Modern Physics* **93**, 15005 (2021).
- [23] Yuto Ashida, Zongping Gong, and Masahito Ueda, “Non-Hermitian physics,” *Advances in Physics* **69**, 249–435 (2020).
- [24] Fabrizio Minganti, Adam Miranowicz, Ravindra W Chhajlany, and Franco Nori, “Quantum exceptional points of non-Hermitian Hamiltonians and Liouvillians : The effects of quantum jumps,” *Physical Review A* **100**, 062131 (2019).
- [25] Ryusuke Hamazaki, “Exceptional dynamical quantum phase transitions in periodically driven systems,” *Nature Communications* **12**, 5108 (2021).
- [26] Kohei Kawabata, Takumi Bessho, and Masatoshi Sato, “Classification of Exceptional Points and Non-Hermitian Topological Semimetals,” *Physical Review Letters* **123**, 66405 (2019).
- [27] Mohammad Ali Miri and Andrea Alù, “Exceptional points in optics and photonics,” *Science* **363**, eaar7709 (2019).
- [28] Wei-chen Wang, Yan-li Zhou, Hui-lai Zhang, Jie Zhang, Man-chao Zhang, Yi Xie, Chun-wang Wu, Ting Chen, Bao-quan Ou, Wei Wu, Hui Jing, and Ping-xing Chen, “Observation of PT -symmetric quantum coherence in a single-ion system,” *Phys. Rev. A* **103**, L020201 (2021).
- [29] Ievgen I. Arkhipov, Adam Miranowicz, Fabrizio Minganti, and Franco Nori, “Raz exceptional points of any order in dissipative linear bosonic systems: Coherence functions and switching between PT and anti-PT symmetries,” *Physical Review A* **102**, 33715 (2020).
- [30] Weijian Chen, Maryam Abbasi, Yogesh N. Joglekar, and Kater W. Murch, “Quantum Jumps in the Non-Hermitian Dynamics of a Superconducting Qubit,” *Physical Review Letters* **127**, 140504 (2021).
- [31] Weijian Chen, Maryam Abbasi, Byung Ha, Serra Erdamar, Yogesh N. Joglekar, and Kater W. Murch, “Decoherence Induced Exceptional Points in a Dissipative Superconducting Qubit,” *Physical Review Letters* **128**, 110402 (2021).
- [32] Parveen Kumar, Kyrylo Snizhko, Yuval Gefen, and Bernd Rosenow, “Optimized steering: Quantum state engineering and exceptional points,” *Physical Review A* **105**, L010203 (2022).
- [33] Wei Nie, Mauro Antezza, Yu Xi Liu, and Franco Nori, “Dissipative Topological Phase Transition with Strong System-Environment Coupling,” *Physical Review Letters* **127**, 250402 (2021).
- [34] Fabrizio Minganti, Alberto Biella, Nicola Bartolo, and Cristiano Ciuti, “Spectral theory of Liouvillians for dissipative phase transitions,” *Physical Review A* **98**, 042118 (2018).
- [35] Álvaro Rubio-García, Ángel L. Corps, Armando Relaño, Rafael A. Molina, Francisco Pérez-Bernal, José Enrique García-Ramos, and Jorge Dukelsky, “Exceptional spectral phase in a dissipative collective spin model,” *Physical Review A* **106**, L010201 (2022).
- [36] Stefano Longhi, “Unraveling the non-Hermitian skin effect in dissipative systems,” *Physical Review B* **102**, 201103(R) (2020).
- [37] Maryam Abbasi, Weijian Chen, Mahdi Naghiloo, Yogesh N. Joglekar, and Kater W. Murch, “Topological Quantum State Control through Exceptional-Point Proximity,” *Physical Review Letters* **128**, 160401 (2022).
- [38] Shishir Khandelwal, Nicolas Brunner, and Géraldine Haack, “Signatures of exceptional points in a quantum thermal machine,” *PRX Quantum* **2**, 040346 (2021).
- [39] J. W. Zhang, J. Q. Zhang, G. Y. Ding, J. C. Li, J. T. Bu, B Wang, L. L. Yan, S. L. Su, L. Chen, F. Nori, K. Özdemir, F. Zhou, H Jing, and M Feng, “Dynamical control of quantum heat engines using exceptional points,” *Nature Communications* **13**, 6225 (2022).
- [40] Akhil Kumar, Kater W. Murch, and Yogesh N. Joglekar, “Maximal quantum entanglement at exceptional points via unitary and thermal dynamics,” *Phys. Rev. A* **105**, 012422 (2021).
- [41] A. Pick, S. Silberstein, N. Moiseyev, and N. Bar-Gill, “Robust mode conversion in NV centers using exceptional points,” *Phys. Rev. Research* **1**, 013015 (2019).
- [42] G. Lindblad, “On the generators of quantum dynamical semigroups,” *Commun. Math. Phys.* **48**, 119–130 (1976).

- [43] Vittorio Gorini, Andrzej Kossakowski, and E. C.G. Sudarshan, “Completely positive dynamical semigroups of N -level systems,” *J. Math. Phys.* **17**, 821–825 (1975).
- [44] Dolf Huybrechts, Fabrizio Minganti, Franco Nori, Michiel Wouters, and Nathan Shammah, “Validity of mean-field theory in a dissipative critical system: Liouvillian gap, PT -symmetric antigap, and permutational symmetry in the XYZ model,” *Physical Review B* **101**, 214302 (2020).
- [45] Tankut Can, Vadim Oganessian, Dror Orgad, and Sarang Gopalakrishnan, “Spectral Gaps and Midgap States in Random Quantum Master Equations,” *Physical Review Letters* **123**, 234103 (2019).
- [46] Victor V Albert and Liang Jiang, “Symmetries and conserved quantities in Lindblad master equations,” *Phys. Rev. A* **89**, 022118 (2014).
- [47] Paolo Zanardi and Lorenzo Campos Venuti, “Geometry, robustness, and emerging unitarity in dissipation-projected dynamics,” *Phys. Rev. A* **91**, 052324 (2015), 1412.6198.
- [48] M Naghiloo, M Abbasi, Yogesh N Joglekar, and K W Murch, “Quantum state tomography across the exceptional point in a single dissipative qubit,” *Nature Physics* **15**, 1232–1236 (2019).
- [49] Serge Haroche and Jean-Michel Raimond, *Exploring the quantum atoms, cavities, and photons* (Oxford University Press, 2010) pp. 205–206.
- [50] Ch. Roos, Th. Zeiger, H. Rohde, H. C. Nägerl, J. Eschner, D. Leibfried, F. Schmidt-Kaler, and R. Blatt, “Quantum state engineering on an optical transition and decoherence in a paul trap,” *Phys. Rev. Lett.* **83**, 4713–4716 (1999).
- [51] A. Kofman and G Kurizki, “Acceleration of quantum decay processes by frequent observations,” *Nature* **405**, 546–550 (2000).
- [52] B. Misra and E. C. G. Sudarshan, “The Zeno’s paradox in quantum theory,” *J. Math. Phys.* **18**, 756–763 (1977).
- [53] M. C. Fischer, B. Gutiérrez-Medina, and M. G. Raizen, “Observation of the quantum zeno and anti-zeno effects in an unstable system,” *Physical Review Letters* **87**, 40402 (2001).
- [54] Tao Chen, Wei Gou, Dizhou Xie, Teng Xiao, Wei Yi, Jun Jing, and Bo Yan, “Quantum Zeno effects across a parity-time symmetry breaking transition in atomic momentum space,” *npj Quantum Information* **7**, 78 (2021).
- [55] P. Facchi, H. Nakazato, and S. Pascazio, “From the quantum zeno to the inverse quantum zeno effect,” *Phys. Rev. Lett.* **86**, 2699–2703 (2001).
- [56] J. Li, T. Wang, L. Luo, S. Vemuri, and Y. N. Joglekar, “Unification of quantum Zeno-anti Zeno effects and parity-time symmetry breaking transitions,” *arXiv: 2004.01364* (2020).
- [57] Florentin Reiter and Anders S. Sørensen, “Effective operator formalism for open quantum systems,” *Physical Review A* **85**, 032111 (2012).
- [58] Li Jiaming, Andrew K. Harter, Ji Liu, Leonardo de Melo, Yogesh N. Joglekar, and Le Luo, “Observation of parity-time symmetry breaking transitions in a dissipative Floquet system of ultracold atoms,” *Nature Communications* **10**, 855 (2019).
- [59] Krzysztof Szczygielski, “On the application of Floquet theorem in development of time-dependent Lindbladians,” *Journal of Mathematical Physics* **55**, 083506 (2014).
- [60] M. Hartmann, D. Poletti, M. Ivanchenko, S. Denisov, and P. Hänggi, “Asymptotic Floquet states of open quantum systems: The role of interaction,” *New Journal of Physics* **19**, 083011 (2017).
- [61] Alexander Schnell, Sergey Denisov, and André Eckardt, “High-frequency expansions for time-periodic Lindblad generators,” *Physical Review B* **104**, 165414 (2021).
- [62] John Gunderson, Jacob Muldoon, Kater W. Murch, and Yogesh N. Joglekar, “Floquet exceptional contours in lindblad dynamics with time-periodic drive and dissipation,” *Physical Review A* **103**, 23718 (2021).
- [63] Claude Cohen-Tannoudji, *Atom-Photon Interactions* (WILEY-VCH Verlag GmbH & Co. KGaA, Weinheim, 2004).
- [64] John Bechhoefer, Avinash Kumar, and Raphaël Chétrite, “A fresh understanding of the Mpemba effect,” *Nature Reviews Physics* **3**, 534–535 (2021).